Obrabotka metallov (tekhnologiya, oborudovanie, instrumenty) = Metal Working and Material Science. 2025 vol. 27 no. 4 pp. 239–256
ISSN: 1994-6309 (print) / 2541-819X (online)
DOI: 10.17212/1994-6309-2025-27.4-239-256

NSTU NETI

Obrabotka metallov - Metal Working and Material Science

Journal homepage: http://journals.nstu.ru/obrabotka_metallov

# Effect of heat treatment on the structure and properties of magnesium alloy MA20 subjected to severe plastic deformation

***Nikita Luginin*** [1, 2, a], ***Anna Eroshenko*** [1, b, *], ***Konstantin Prosolov*** [1, c], ***Margarita Khimich*** [1, d], ***Ivan Glukhov*** [1, e], ***Alexander Panfilov*** [1, f], ***Alexey Tolmachev*** [1, g], ***Pavel Uvarkin*** [1, h], ***Alexander Kashin*** [1, i], ***Yurii Sharkeev*** [1, 2, j]

[1] Institute of Strength Physics and Materials Sciences SB RAS, 2/4 per. Academicheskii, Tomsk, 634055, Russian Federation
[2] National Research Tomsk Polytechnic University, Lenin Ave., 30, Tomsk, 634050, Russian Federation

[a] https://orcid.org/0000-0001-6504-8193, nikishek90@ispms.ru; [b] https://orcid.org/0000-0001-8812-9287, eroshenko@ispms.ru;
[c] https://orcid.org/0000-0003-2176-8636, konstprosolov@ispms.ru; [d] https://orcid.org/0000-0001-5859-7418, khimich@ispms.ru;
[e] https://orcid.org/0000-0001-5557-5950, gia@ispms.ru; [f] https://orcid.org/0000-0001-8648-0743, alexpl@ispms.ru;
[g] https://orcid.org/0000-0003-4669-8478, tolmach@ispms.ru; [h] https://orcid.org/0000-0003-1169-3765, uvarkin@ispms.ru;
[i] https://orcid.org/0000-0003-1860-3654, kash@ispms.ru; [j] https://orcid.org/0000-0001-5037-245X, sharkeev@ispms.ru

**ARTICLE INFO**

*Article history*:
Received: 29 July 2025
Revised: 03 September 2025
Accepted: 12 September 2025
Available online: 15 December 2025

*Keywords*:
Magnesium alloys
Severe plastic deformation
Mechanical properties
Heat treatment
Phase composition
Structure

*Funding*
The Russian Science Foundation has financially supported the work, project No. 23-13-00359, available online: https://rscf.ru/project/23-13-00359/. The investigations have been carried out using the equipment of Share Use Centre "Nanotech" of the ISPMS SB RAS and at core facility "Structure, mechanical and physical properties of materials" NSTU.

**ABSTRACT**

**Introduction.** One of the most promising fields for the application of magnesium alloys is medicine. Their key advantages are bioresorbability and a low elastic modulus, comparable to that of human cortical bone (up to 30 GPa). Biocompatible *Mg-Zn-Zr-Ce* (*MA20*) system alloys are among the most promising for medical applications. Due to their relatively low mechanical properties, the development of severe plastic deformation (*SPD*) techniques for forming an ultrafine-grained (*UFG*) state in bulk billets of the *Mg-Zn-Zr-Ce* alloy to achieve optimal functional properties requires further research. Analyzing the conditions for forming a high-strength *UFG* state necessitates considering various strengthening mechanisms, including well-known ones related to the effect of *UFG* structures. Identifying the deformation and strain hardening mechanisms in magnesium alloys subjected to *SPD* is also highly relevant. The **purpose of this work** is to establish the mechanisms of strain hardening and to investigate the influence of heat treatment on the structure and properties of the *MA20* magnesium alloy after combined *SPD*. **Research methods.** The study object was the *MA20* alloy in a *UFG* state (wt. %: *Mg* – 98.0; *Zn* – 1.3; *Ce* – 0.1; *Zr* – 0.1; *O* – 0.5). The *UFG* state was achieved via a combined *SPD* process involving *ABC*-pressing followed by multi-pass rolling in grooved rolls. To study the effect of annealing on the microstructure and mechanical tensile properties, samples were annealed in air at temperatures of 200, 250, 300, and 500 °C for 24 hours. The microstructure and phase composition of the samples were investigated using optical and transmission electron microscopy. **Results and discussion.** It was established that applying a combined *SPD* method (*ABC*-pressing and multi-pass rolling) to the *MA20* alloy results in the formation of an ultrafine-grained structure with an average grain size of about 1 μm. This leads to a significant increase in yield strength ($\sigma_{0.2}$) to 250 MPa and ultimate tensile strength ($\sigma_u$) to 270 MPa, while simultaneously reducing ductility to 3%. Annealing at 200 °C was found to preserve the *UFG* state in the *MA20* alloy and to lead to a 100% increase in ductility, with an 8% decrease in $\sigma_{0.2}$ and a 4% decrease in $\sigma_u$ compared to the initial *UFG* state (non-annealed). ***Conclusions***. It was revealed that the grain boundary ($\sigma_{grain}$ = = 202 MPa) and dislocation ($\sigma_{dis}$ = 69 MPa) strengthening contributions provide the most significant increase in the strength of the *UFG MA20* magnesium alloy. For the magnesium alloy in the *UFG* and fine-grained (*FG*) states, a critical grain size interval of (1–7) μm was identified, corresponding to a sharp increase in the intensity of change for the calculated contributions of dislocation ($d\sigma_{dis}/dd$), grain boundary ($d\sigma_{grain}/dd$), overall strengthening ($d\sigma_{total}/dd$), and dislocation density ($d\rho/dd$). For the coarse-grained (*CG*) state of the alloy in the grain size range (7–40) μm, these parameters stabilize.

**For citation:** Luginin N.A., Eroshenko A.Yu., Prosolov K.A., Khimich M.A., Glukhov I.A., Panfilov A.O., Tolmachev A.I., Uvarkin P.V., Kashin A.D., Sharkeev Yu.P. Effect of heat treatment on the structure and properties of magnesium alloy MA20 subjected to severe plastic deformation. *Obrabotka metallov (tekhnologiya, oborudovanie, instrumenty) = Metal Working and Material Science*, 2025, vol. 27, no. 4, pp. 239–256. DOI: 10.17212/1994-6309-2025-27.4-239-256. (In Russian).

*** Corresponding author**
*Eroshenko Anna Yu.,* Ph.D. (Engineering), Senior Researcher
Institute of Strength Physics and Materials Science SB RAS,
2/4 per. Academicheskii,
634055, Tomsk, Russian Federation
**Tel.:** +7 3822 286 911, **e-mail**: eroshenko@ispms.ru

## Introduction

One of the most promising areas for the use of magnesium alloys is considered to be medicine [1]. Their key advantages are bioresorbability and a relatively low elastic modulus, comparable to that of human cortical bone (up to 30 GPa). The matching of the elastic moduli of bone tissue and the magnesium alloy eliminates high stresses at the bone-implant interface [2]. Magnesium and its alloys have the ability to undergo bioresorption, making them useful for certain types of orthopedic and vascular surgeries. The resorption of a magnesium implant and its replacement by bone tissue in the body during treatment avoids the need for repeated surgical intervention. The disadvantages of magnesium alloys include low corrosion resistance and the release of hydrogen during metal corrosion [3]. Furthermore, for some implants subjected to load-bearing applications, the level of strength properties does not meet the necessary requirements. Alloying magnesium with specific elements can reduce the resorption rate of the implanted device, thereby increasing corrosion resistance, as well as enhance mechanical strength while maintaining satisfactory ultimate plasticity.

Elements considered favorable for medical applications include Ca, Mn, Zn, Sn, Sr, and Ce [4]. The most promising for medical applications are alloys based on the Mg-Zn-Zr system. The addition of Ce up to 0.3 wt. % to the Mg-Zn-Zr system improves plasticity [5]. Microalloying with Ce leads to the formation of finer and more spherical intermetallic compounds, which promote the nucleation of crystallization sites and refine the average grain size [6].

In magnesium alloys, an enhancement of mechanical properties can be achieved by refining the grain structure using methods of severe plastic deformation (SPD) [7]. This approach allows for a 2 to 2.5-fold increase in strength properties without the introduction of additional alloying elements, due to the formation of an ultrafine-grained (UFG) structure.

To date, there are publications presenting research results on the structure [5] and mechanical properties [8] of Mg-Zn-Zr system alloys with additions of Ce and Ca in various structural states [9]. However, despite a number of publications [1,3,4,10-12] dedicated to achieving an ultrafine-grained (UFG) state in magnesium alloys via SPD methods, the problem of obtaining an average grain size of less than 1 μm still remains. Furthermore, there is a need to identify regimes for the subsequent thermal treatment of magnesium alloy products to relieve residual internal stresses and enhance plasticity while simultaneously preserving the UFG structure of the alloy. UFG and fine-grained (FG) states in magnesium alloys are characterized by relatively low plasticity and limited fatigue endurance. This is associated with the peculiarities of their hexagonal close-packed (HCP) lattice, in which deformation occurs primarily through slip on basal planes, significantly reducing the workability of products and semi-finished workpieces made from such alloys.

At room temperature, two main deformation mechanisms are realized in magnesium alloys: basal slip and twinning [13]. An increase in temperature during deformation leads to the activation of several slip planes: basal {0001}, prismatic {1010}, pyramidal {1122}, and twinning {1012}, and consequently, to an increase in the plasticity of magnesium after deformation processing [14]. Therefore, the pressure treatment of magnesium and its alloys is conducted at temperatures of 250-430 °C, which allows for the activation of prismatic and pyramidal slip systems [15], as well as secondary twinning [16]. A study of the deformation behavior of magnesium and its alloys in [17] showed that at temperatures below 225 °C, the primary deformation mechanism is twinning, which usually leads to a sharp drop in plasticity.

It is known that the UFG structure formed by SPD methods in metals and alloys has its own specific features associated with the small grain size, high lattice curvature, extensive non-equilibrium grain boundaries, etc., which leads to a significant increase in the strength of materials [18]. Furthermore, the use of SPD methods promotes the segregation of alloying elements at grain boundaries and the formation of fine dispersoids of secondary phases [19]. In combination with the ultrafine-grained structure, this provides an additional contribution to the enhancement of the strength characteristics of metals. In this regard, research aimed at analyzing the influence of various strengthening mechanisms on strength properties, including UFG alloys, is of particular relevance.

For magnesium alloys, strengthening mechanisms have been studied in works [12,20]. Study [12] established that in the Mg-1Zn-0.2Ca alloy, microalloying with Zn and Ca promotes the realization of the

grain boundary strengthening mechanism by refining the structure to an FG state during multi-directional isothermal forging. This made it possible to significantly increase the mechanical properties in tensile tests, raising the yield strength to 210 MPa, the ultimate tensile strength to 260 MPa, and the elongation to failure to 20 %.

The authors of [21] investigated the effect of extrusion on the microstructure of an Mg-Y-Gd-Zr alloy, which was additionally alloyed with Sm and Gd. It was found that the reduction in grain size is related to the magnitude of accumulated strain. The study also investigated the influence of the Sm addition on the kinetics of the decomposition of the magnesium solid solution in the Mg-Y-Gd-Zr alloy in the deformed state. It was shown that after deformation, the Mg-Y-Gd-Zr and Mg-Y-Gd-Sm-Zr alloys were additionally strengthened by the solid solution mechanism.

In work [20], a significant contribution of strain hardening to the overall strength of an alloy from the Mg-Zn-Ca system was identified. It is shown that the application of a combined SPD method allows for a reduction of the average grain size from 220 to 20 μm, thereby increasing the ultimate strength of the alloy from 144 to 233 MPa.

To analyze the conditions for the formation of a high-strength state in UFG alloys, it is necessary to account for various strengthening mechanisms, including well-known ones associated with the influence of UFG structures. Therefore, the issues of identifying the deformation and strain hardening mechanisms of magnesium alloys formed under severe deformation conditions require further investigation.

***The aim of this work*** was to establish the mechanisms of strain hardening in MA20 alloy subjected to combined SPD and to determine the influence of heat treatment on its structure and properties. To achieve this aim, the following ***research tasks*** were set:

1. To evaluate the grain size in MA20 alloy after the application of the SPD method.
2. To perform mechanical testing of alloy samples in various states to assess the strength and plasticity of the alloy.
3. To evaluate the contributions of various strengthening mechanisms (grain boundary, dislocation, etc.) to the yield strength of the alloy under different thermal treatments.
4. To determine the grain size interval at which a change in the strain hardening mechanisms of MA20 magnesium alloy occurs.

## Research methodology

The object of the study was the commercial magnesium alloy (MA20) of the Mg-Zn-Zr-Ce system, developed at the All-Russian Scientific Research Institute of Aviation Materials (Moscow, Russia). The magnesium alloy billet was produced by remelting at the All-Russian Institute of Light Alloys (Moscow, Russia, JSC VILS) followed by hot rolling to a plate thickness of 30 mm. The alloy had the following composition (wt. %): Mg – 98.0; Zn – 1.3; Ce – 0.1; Zr – 0.1; O – 0.5.

The UFG state in MA20 magnesium alloy was achieved using a combined SPD method, consisting of 3abc pressing and multi-pass rolling [22]. At the 3abc pressing stage, the billet was pressed in a die at a temperature of 250 °C, being rotated by 90° after each pressing cycle. The total logarithmic strain for all pressing stages amounted to 1.1. Rolling of the samples, preheated to 250 °C, was carried out at room temperature to a total logarithmic strain of 1.5.

To investigate the influence of the final heat treatment temperature on the mechanical properties of the magnesium alloy, samples in the UFG state were annealed at temperatures of 200, 250, and 300 °C for 24 hours in a SNOL 10/11 muffle furnace and cooled in air. The selected temperature-time regimes of thermal treatment ensured a low rate of diffusion processes in the magnesium alloys [23]. For the complete relaxation of stresses, the initial alloy was annealed at a temperature of 500 °C for 8 hours in a SNOL 10/11 muffle furnace followed by cooling in air.

The microstructure of the obtained billets was studied using an optical microscope (Altami MET 1 MT, St. Petersburg, Russia) and a transmission electron microscope (TEM) (JEOL JEM 2100 electron microscope, Tokyo Boeki Ltd., Tokyo, Japan) equipped with an energy-dispersive X-ray spectroscopy

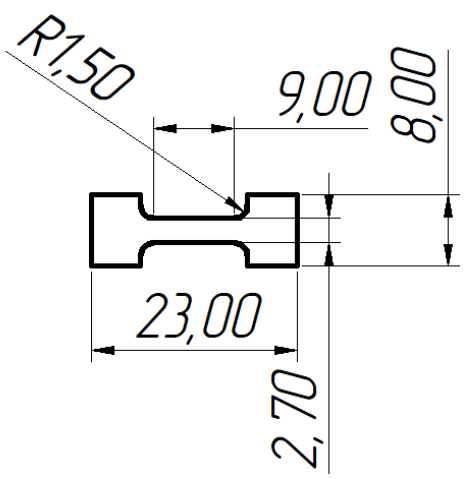


*Fig. 1.* Schematic representation of specimens for mechanical tensile testing

(EDS) attachment. The elemental composition of the samples prior to deformation was determined using a Niton XL3t X-ray fluorescence analyzer (Thermo Scientific, Massachusetts, USA).

Microhardness measurements were conducted using the Vickers method on a Duramin-5 tester (Struers, Ballerup, Denmark). The yield strength, ultimate tensile strength, and maximum elongation were determined during tensile tests using a UTS-110M-100 testing machine (Test-Sistemy, Ivanovo, Russia). For these tests, flat "dog-bone" shaped specimens with the following working dimensions were used: thickness – 3.0 mm, width – 2.7 mm, length – 9.0 mm. A diagram of the specimens for mechanical testing is presented in Figure 1. The specimens were manufactured using the wire electrical discharge machining (EDM) method.

Sample preparation for transmission electron microscopy (TEM) was performed by cutting the billets into 0.3 mm thick plates using electrical discharge machining (EDM), which were then mechanically thinned to a thickness of 0.1 mm on P2500 grit sandpaper. Further sample preparation was carried out by ion milling using an ion mill (JEOL Ion Slicer EM-09100IS, Tokyo Boeki Ltd., Tokyo, Japan). Interplanar spacing data were calculated from microdiffraction patterns using the Crystallography Open Database (COD) as of 21.01.2025. The average size (of grains, subgrains, fragments) was determined by the linear intercept method. The scalar dislocation density was determined by the linear intercept method using bright-field TEM images and the following formula [24]:

$$< \rho >= \frac{1}{t} \cdot \left( \frac{N_1}{L_1} + \frac{N_2}{L_2} \right), \quad (1)$$

where $t$ = 150 nm is the foil thickness; $N_1$ and $N_2$ are the total numbers of intersections of dislocations with the horizontal and vertical lines, respectively, drawn on the bright-field TEM image; $L_1$ and $L_2$ are the total lengths of all horizontal and vertical lines, respectively, drawn on the bright-field TEM image, nm.

Additionally, the types of dislocation substructures were determined based on the corresponding values of scalar dislocation density and electron microscopy images of the regions of the studied samples. The assessment of the contributions of various mechanisms to the strain hardening of the alloy for the investigated structural states was performed according to the methodology presented in [19].

Subsequently, dependencies of dislocation density and the contributions of strengthening mechanisms on the average grain size were plotted. The obtained dependencies were differentiated, and the derivatives were plotted, characterizing the intensity of change in the contributions of the strengthening mechanisms, the total stress, and the dislocation density with respect to the grain size.

## Results and Discussion

Figure 2a shows an optical image of the microstructure of MA20 magnesium alloy in the initial coarse-grained (CG) state. The alloy's microstructure consists of equiaxed grains based on an α-solid solution of alloying elements in magnesium. The average grain size, determined by the linear intercept method, was 25.0 ± 10.0 μm. A large number of predominantly spherical particles and regions of particle accumulation are observed inside the grains, which are uniformly distributed within the grains.

According to literature data, in alloys of the Mg-Zn-Zr-Ce system, these particles are identified as nanoscale intermetallic compounds $MgZn_2$, $CeZn_3$, and $Ce_3Zn_{11}$ [25]. Furthermore, the alloys contain larger particles ranging from 2 to 10 μm, which are zirconium and cerium hydrides ($ZrH_2$ and $Ce_2H_5$) [22].

During deformation, hydride particles can acquire additional mobility, which, in turn, leads to their further agglomeration in the process of deformation, affecting the level of mechanical properties. Thus, the authors of [26] established the role of the influence of hydrides and dissolved hydrogen in the magnesium

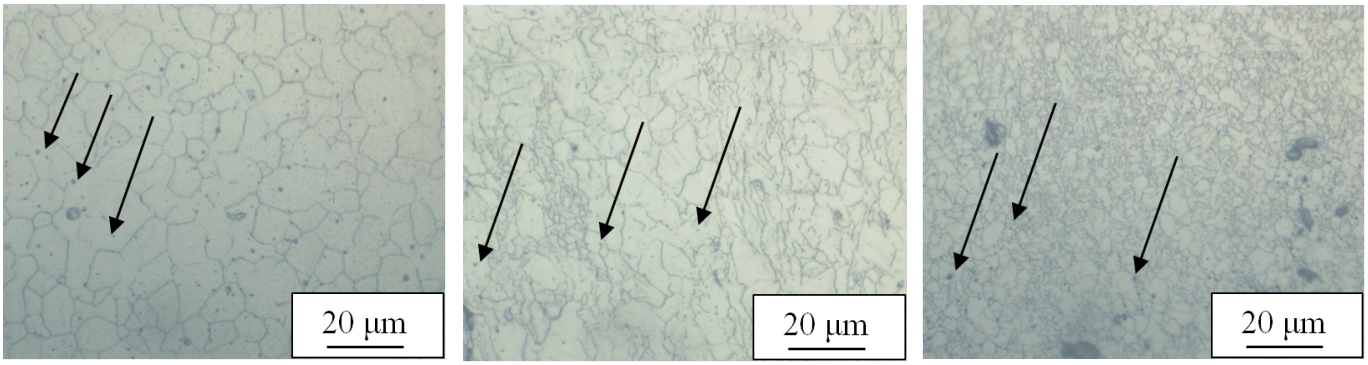


*a* *b* *c*

*Fig. 2.* Optical images of the microstructure of the *MA20* alloy in different states: *a – CG*; *b – FG*; *c – UFG*. Particles of hydrides and intermetallics are indicated by arrows

matrix on the mechanical properties of Mg-Al, Mg-Zn, Mg-Ca, and Mg-RE alloy systems. It was shown that hydrides reduce the mechanical properties of magnesium alloys because they act as sinks for dislocations, leading to crack formation. Hydrides also agglomerate during deformation. This reduces the material's plasticity and is a significant drawback that limits the practical application of magnesium alloys [27]. A more detailed description of the microstructure of the MA20 alloy was provided by the authors of this study in work [22].

The average grain size decreases after deformation by 3abc pressing. After 3abc pressing, a fine-grained (FG) state is formed with an average grain size of 3.0 ± 1.5 μm (Figure 2b). The fraction of hydride and intermetallic particles remains unchanged after the deformation processing. Most grains are non-equiaxed and have an irregular shape. Subsequent deformation by rolling promoted additional refinement of the primary phase microstructure to 1.0 ± 0.7 μm (Figure 2c), which corresponds to an ultrafine-grained (UFG) state. According to optical metallography data (Figure 2), deformation by rolling leads to the agglomeration of particles and hydrides, which may indicate their high mobility during SPD [28].

The results of TEM studies of the alloy's microstructure in the CG state are presented in Figure 3. Bright-field TEM images show equiaxed grains of the primary phase based on an α-solid solution of alloying elements in magnesium (HCP lattice) and particle inclusions (Figure 3a, d). As a result of microdiffraction analysis, the intermetallic compounds $MgZn_2$, $CeZn_3$, and $Ce_3Zn_{11}$ were identified in the CG alloy (Figure 3b, e). Figure 3a, c, d, e present dark-field and bright-field images of $MgZn_2$, $CeZn_3$, and $Ce_3Zn_{11}$ particles.

Additionally, EDS analysis was performed, which showed that in $MgZn_2$ particles, the ratio of magnesium to zinc (at. %) is 1.5:2, which corresponds to the stoichiometric composition of the intermetallic compound, since magnesium is the primary phase in the alloy. For the $CeZn_3$ and $Ce_3Zn_{11}$ intermetallics, the element ratios (at. %) are 1:3.5 and 1:4, respectively, which are close to the stoichiometric compositions of the particles.

According to the Mg-Zn [29] and Zn-Ce [30] phase diagrams, the indicated intermetallic compounds are stable and exist at room temperature. It should be noted that intermetallic compounds can significantly influence deformation processes by inhibiting grain boundary motion [19].

After *abc*-pressing, subgrains form inside the matrix grains (Figure 4a). A network dislocation substructure forms inside the subgrains (Figure 4b, c) with a scalar dislocation density of $5 \cdot 10^9$ $cm^{-2}$. The phase composition of the alloy in the FG state corresponds to that of the alloy in the CG state. The alloy contains intermetallic compounds $MgZn_2$, $CeZn_3$, and $Ce_3Zn_{11}$, as well as a certain amount of zirconium hydride $ZrH_2$ and cerium hydride $Ce_2H_5$, which was confirmed by SEM studies and X-ray phase analysis by the authors in a previous work [22].

Combined SPD (*abc*-pressing + rolling) leads to the formation of a UFG structure with an average grain size of 1.0 ± 0.7 μm. TEM images reveal a cellular-network dislocation substructure (Figure 5b, c) with a scalar dislocation density of $2 \cdot 10^{10}$ $cm^{-2}$. The phase composition of the alloy did not change qualitatively after the combined SPD.

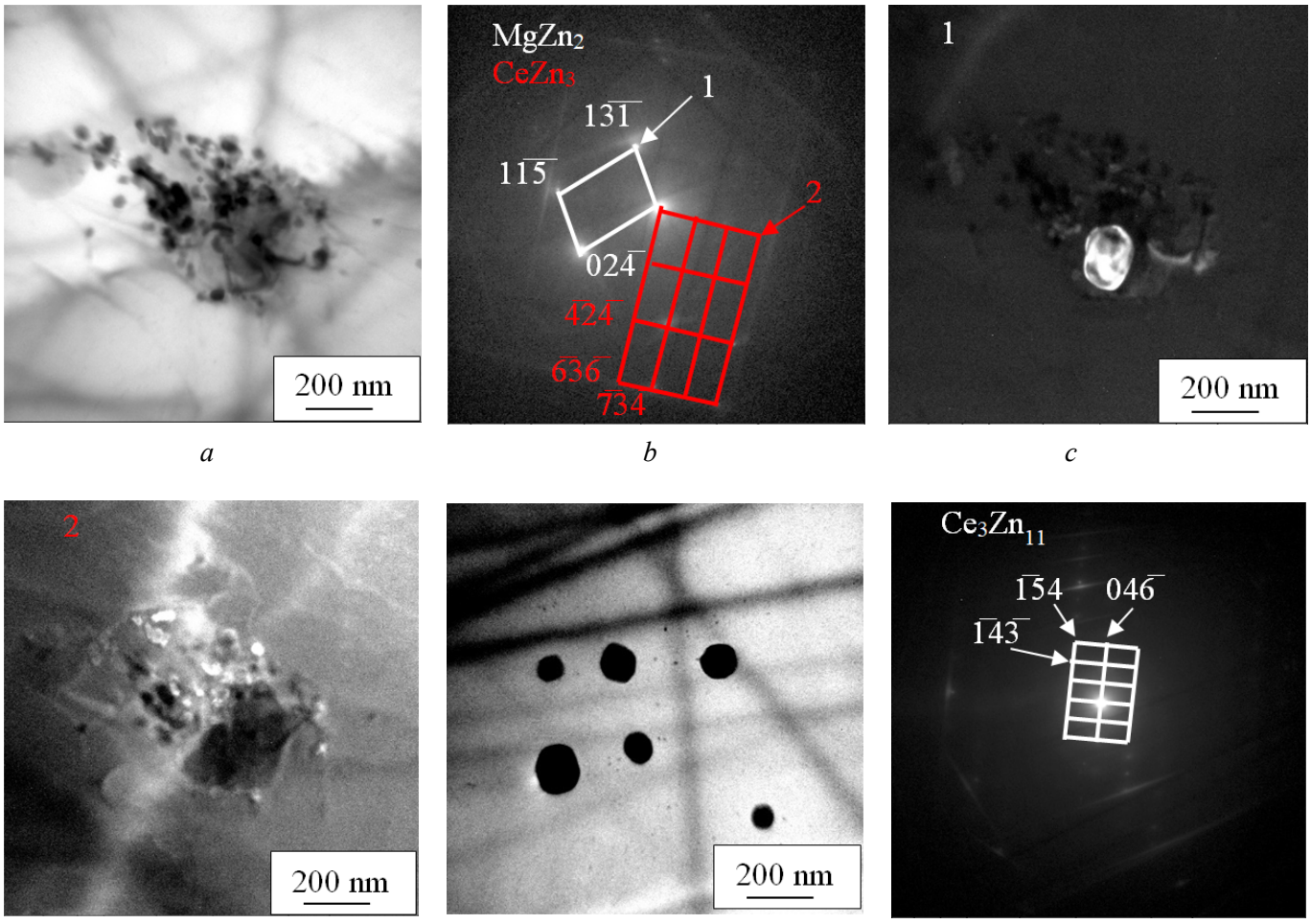


*a* *b* *c*

*d* *e* *f*

*Fig. 3.* TEM images of the microstructure of the magnesium alloy in the *CG* state:

*a*, *e* – bright-field image of particles $MgZn_2$, $CeZn_3$ and $Ce_3Zn_{11}$; *b*, *f* – microdiffraction pattern from intermetallic compounds $MgZn_2$, $CeZn_3$ and $Ce_3Zn_{11}$; *c*, *d* – dark-field image of particles $MgZn_2$ and $CeZn_3$

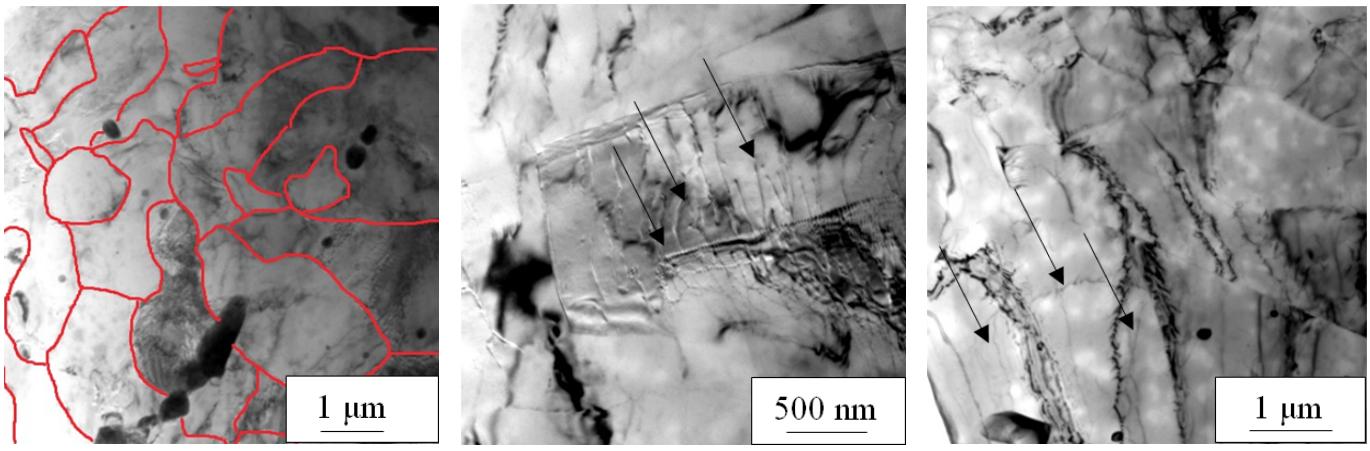


*a* *b* *c*

*Fig. 4. TEM* images of *MA20* alloy in the *FG* state:

*a* – bright-field image of the alloy grain structure; *b*, *c* – bright-field image of the dislocation substructure. Network dislocation structure is indicated by arrows

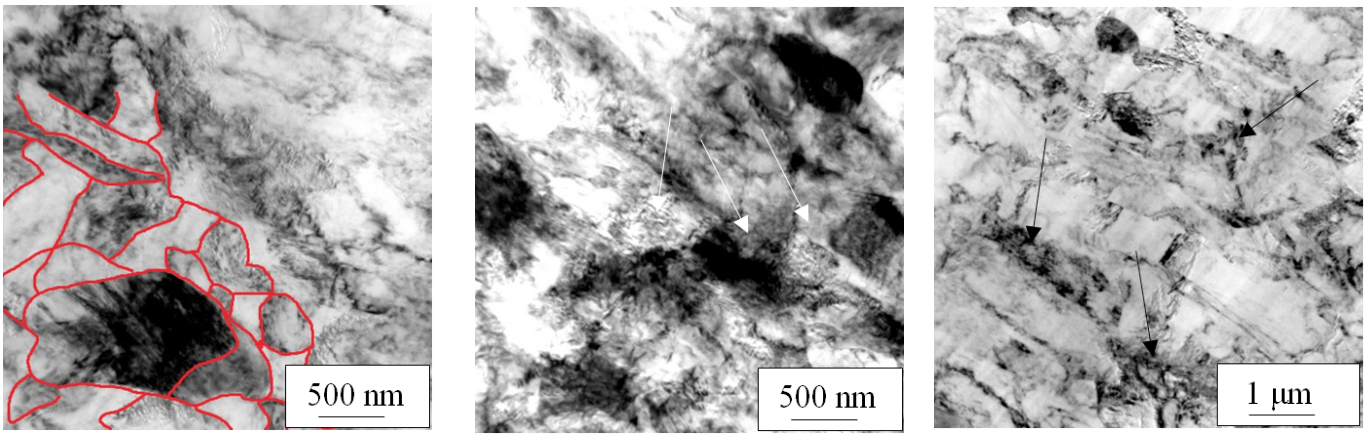


*a* *b* *c*

*Fig. 5.* Bright-field *TEM* images of *MA20* alloy in the *UFG* state:
*a* – subgrain structure; *b*, *c* – cellular-network dislocation substructure. Arrows indicate the dislocation substructure

At the next stage, microstructural studies were conducted for the UFG alloy samples after annealing for 24 hours at temperatures of 200, 250, and 300 °C. Optical images of the microstructure of the UFG alloy subjected to heat treatment at various temperatures are presented in Figure 6.

Based on the results of optical microscopy, it was established that annealing the magnesium alloy in the UFG state at a temperature of 200 °C preserves the UFG state of the alloy. Annealing at 250 and 300 °C increases the average grain size to 1.5 ± 0.8 μm and 7.0 ± 5.0 μm, respectively, transitioning the alloy into the FG state.

TEM images of the alloy's microstructure after thermal treatment are presented in Figure 7. The results of TEM studies confirm the optical microscopy data. Annealing at 200 °C leads to a decrease in dislocation density in the alloy from $2 \cdot 10^{10}$ to $9 \cdot 10^{9}$ $cm^{-2}$; however, the dislocation substructure remains largely unchanged – cellular-network (Figure 7a). An increase in the annealing temperature to 250 °C leads to an increase in grain size and a further decrease in the scalar dislocation density to $6 \cdot 10^{9}$ $cm^{-2}$; the dislocation structure becomes a network with a chaotic distribution of dislocations within it (Figure 7b). The TEM images show that the alloy's structure becomes more homogeneous throughout the volume, which indicates the onset of recrystallization processes. A further increase in the annealing temperature to 300 °C leads to more intense recrystallization processes in the alloy and a substantial increase in grain size. The network dislocation structure transforms into individual dislocation clusters. The dislocation density decreases to $4 \cdot 10^{9}$ $cm^{-2}$ (Figure 7c).

After annealing at 200 °C, the dislocation density was found to be $9 \times 10^{9}$ $cm^{-2}$, which is lower than that of the UFG state ($2 \cdot 10^{10}$ $cm^{-2}$). An increase in the annealing temperature to 250 and 300 °C reduces the

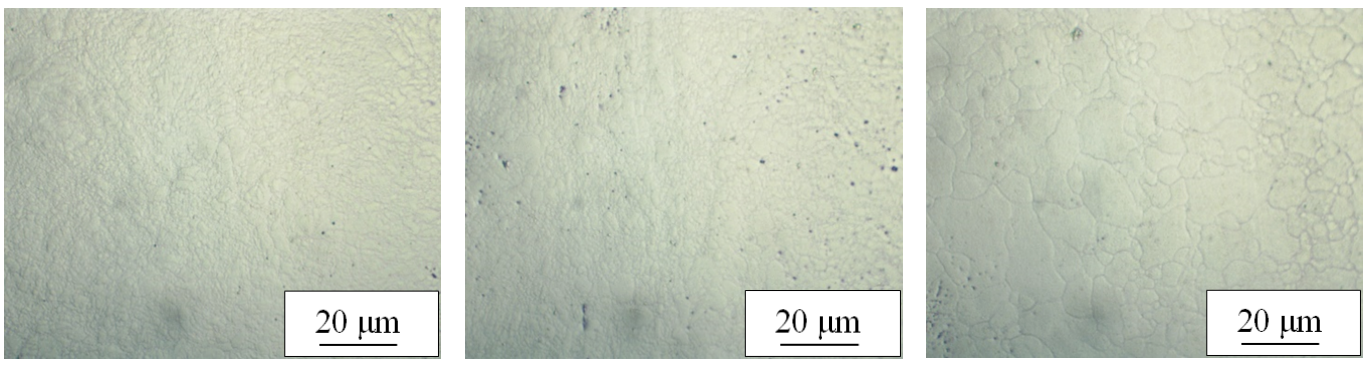


*a* *b* *c*

*Fig. 6.* Optical images of the structure of the *UFG* alloy after heat treatment:
*a* – 200 °C; *b* – 250 °C; *c* – 300 °C

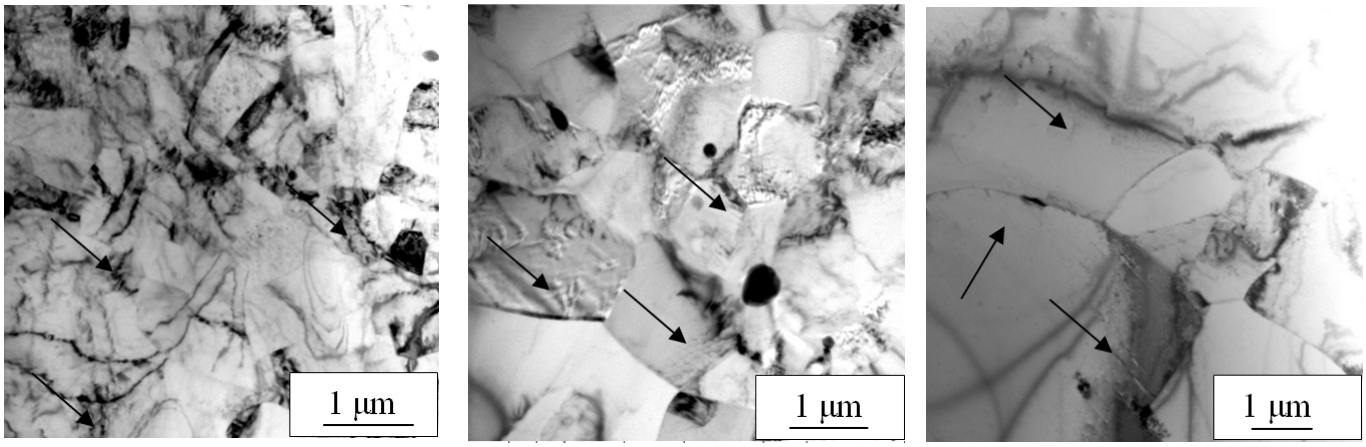


*a* *b* *c*

*Fig. 7.* Bright-field *TEM* images of the microstructure of the *UFG* alloy after heat treatment:
*a* – 200 °C, cellular-network dislocation structure; *b* – 250 °C, network dislocation structure; *c* – 300 °C, dislocation clusters and tangles. Arrows indicate the dislocation substructure

scalar dislocation density to $6 \cdot 10^9$ $cm^{-2}$ (annealing at 250 °C) and further to $4 \cdot 10^9$ $cm^{-2}$ (annealing at 300 °C), respectively, due to the activation of the recovery process [31].

Figure 8 shows the microstructure of the coarse-grained (initial) alloy after annealing at 500 °C. In this state, the structure has a distinct granular character and consists of equiaxed α-grains based on a magnesium solid solution (Figure 8a). The average grain size was 40.0 ± 15.0 μm. Furthermore, a small number of intermetallic particles of secondary phases, which did not dissolve during the annealing process, are observed along the grain boundaries.

Figure 9a presents the tensile stress-strain curves of the alloy samples. Mechanical testing showed that the UFG sample has the maximum values of yield strength and ultimate tensile strength ($\sigma_{0.2}$ = 250 MPa and $\sigma_{UTS}$ = 270 MPa) compared to the FG ($\sigma_{0.2}$ = 40 MPa and $\sigma_{UTS}$ = 220 MPa) and CG ($\sigma_{0.2}$ = 250 MPa and $\sigma_{UTS}$ = 190 MPa) states. The ultimate plasticity of the alloy for the UFG, FG, and CG states was 3%, 9%, and 13%, respectively.

Heat treatment of the alloy in the UFG state leads to a decrease in strength properties and an increase in the plasticity of the alloy (Figure 9b). Annealing at a temperature of 200 °C results in a 100% increase in plasticity and the achievement of high strength without changing the grain size. In this case, $\sigma_{0.2}$ and $\sigma_{UTS}$ decrease slightly – by 8% and 4%, respectively – compared to the UFG state (without annealing). Fur-

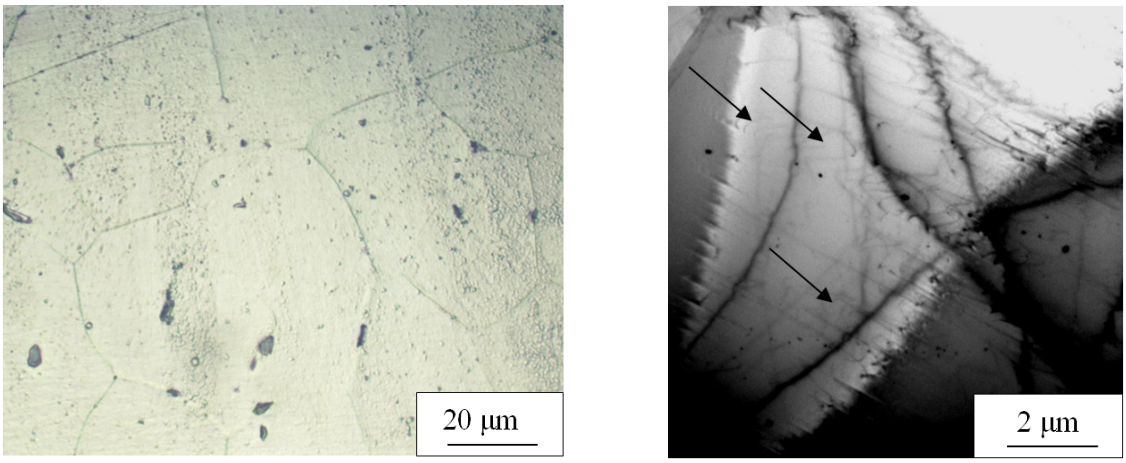


*a* *b*

*Fig. 8.* Optical (*a*) and bright-field *TEM* (*b*) images of the alloy microstructure after annealing at 500 °C. Arrows indicate the dislocation substructure

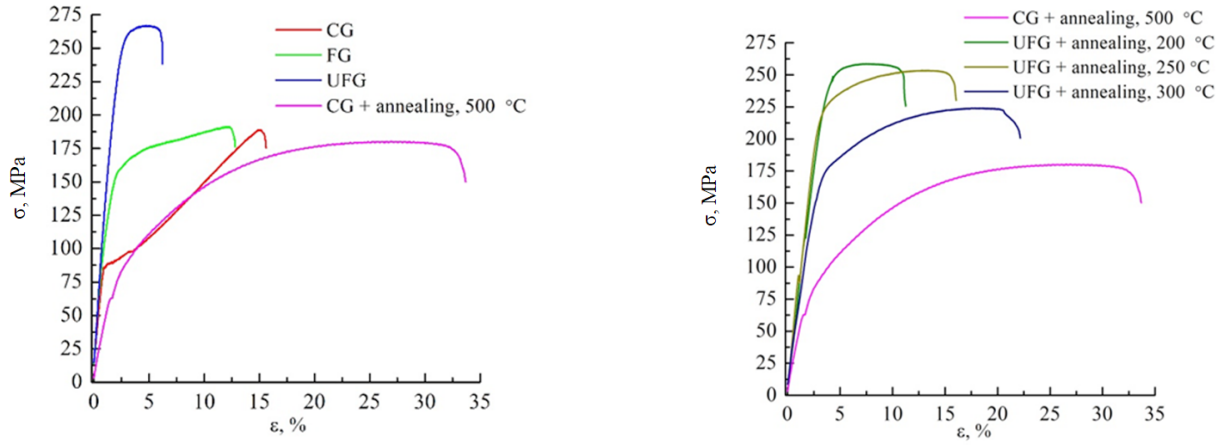


*a* *b*

*Fig. 9.* Stress-strain curves in different structural states (*a*) and after annealing at 500, 300, 250 and 200 °C (*b*)

ther annealing of the alloy at 250 °C leads to an increase in ultimate plasticity and a decrease in the yield strength. Subsequently, annealing at 300 °C also results in a decrease in strength properties and an increase in ultimate plasticity due to a reduction in defect density and recrystallization.

High-temperature annealing (500 °C) of the alloy in the CG state, which was applied for the complete relaxation of internal stresDses, is characterized by active recrystallization, which leads to a sharp decrease in strength and the achievement of the highest plasticity.

Table 1 presents data on the influence of grain size on the mechanical properties of the alloy. To identify the main strengthening mechanisms in the magnesium alloy, an assessment of the contributions of the active

Table 1

**Mechanical and structural properties of MA20 alloy**

| Number | Alloy state | Average grain size, μm | $\sigma_{0,2}$, MPa | $\sigma_{UTS}$, MPa | δ, % | Scalar dislocation density, <ρ>, $cm^{-2}$ Dislocation substructure type |
|---|---|---|---|---|---|---|
| 1 | CG + annealing, 500 °C | 40,0±15,0 | 60 | 180 | 25 | $8 \cdot 10^8$ Individual dislocations and dislocation clusters |
| 2 | CG | 25,0±10,0 | 90 | 190 | 13 | $4 \cdot 10^9$ Dislocation clusters |
| 3 | UFG + annealing, 300 °C | 7,0±5,0 | 150 | 220 | 17 | $4 \cdot 10^9$ Dislocation clusters and tangles |
| 4 | FG | 3,0±2,0 | 140 | 220 | 9 | $5 \cdot 10^9$ Network dislocation substructure |
| 5 | UFG + annealing, 250°C | 1,5±0,8 | 210 | 250 | 11 | $6 \cdot 10^9$ Network dislocation substructure and dislocation clusters |
| 6 | UFG + annealing, 200 °C | 1,0±0,7 | 230 | 260 | 6 | $9 \cdot 10^9$ Network dislocation substructure |
| 7 | UFG | 1,0±0,7 | 250 | 270 | 3 | $2 \cdot 10^{10}$ Cellular-network dislocation substructure |

Note: $\sigma_{0,2}$ – yield strength, $\sigma_{UTS}$ – ultimate tensile strength, δ – elongation to failure.

strengthening mechanisms to the yield strength of the magnesium alloy was carried out [19,32]. This work involved the calculation of the additive contributions of strengthening mechanisms, such as the lattice friction stress, dislocation strengthening, and grain boundary strengthening, to the yield strength of the alloy:

$$\sigma_{total} = \sigma 0 + \sigma_{dis} + \sigma_{gb}, \quad (2)$$

where $\sigma_{total}$ is the calculated yield strength of the alloy; $\sigma_0$ is the stress due to dislocation slip in a single crystal, as well as solid solution and dispersion strengthening; $\sigma_{dis}$ is dislocation strengthening; $\sigma_{gb}$ is grain boundary strengthening.

It is known that the primary strengthening mechanism in UFG metals and alloys is grain boundary strengthening, described by the Hall-Petch equation [18,19,33]. The mechanisms of strain hardening in magnesium alloys also include dislocation slip and twinning [34]. Study [35] demonstrated that the primary strengthening mechanism in samples of extruded AZ31 alloy under cyclic deformation according to a "compression-tension" scheme is twinning. Typically, active twinning in magnesium alloys promotes effective grain refinement even at low strains. Study [36] investigated a ZK60 alloy in the FG state (average grain size – 3 μm), produced by extrusion. It was established that the alloy deforms through twinning and basal slip at high strain rates ($\varepsilon = 10^3$ $s^{-1}$); however, at lower rates ($\varepsilon = 10^1$ $s^{-1}$), the twinning mechanism is suppressed, leading to a sharp decrease in the plasticity of the magnesium alloy.

In study [37], grain boundary strengthening for the magnesium alloy was determined using the Hall-Petch relationship:

$$\sigma_{gb} = Kd^{-1/2}, \quad (3)$$

where K is the Hall-Petch constant; d is the average grain size of the primary phase. Based on the obtained experimental data (Table 1), the dependence of the yield strength $\sigma_{0.2}$ on $d^{-1/2}$ was plotted (Figure 10). In the grain size interval of (1-40) μm, the dependence of $\sigma_{0.2}$ on $d^{-1/2}$ is linear ($K = 202$ MPa·μm$^{1/2}$). In accordance with the Hall-Petch relationship, for the studied alloy, the value of $\sigma_{gb}$ is 40 MPa.

The contribution of the dislocation structure to the material's strengthening was calculated using the Taylor equation [38]:

$$\sigma_{dis} = b \cdot \div \cdot G \cdot \sqrt{<\rho>}, \quad (4)$$

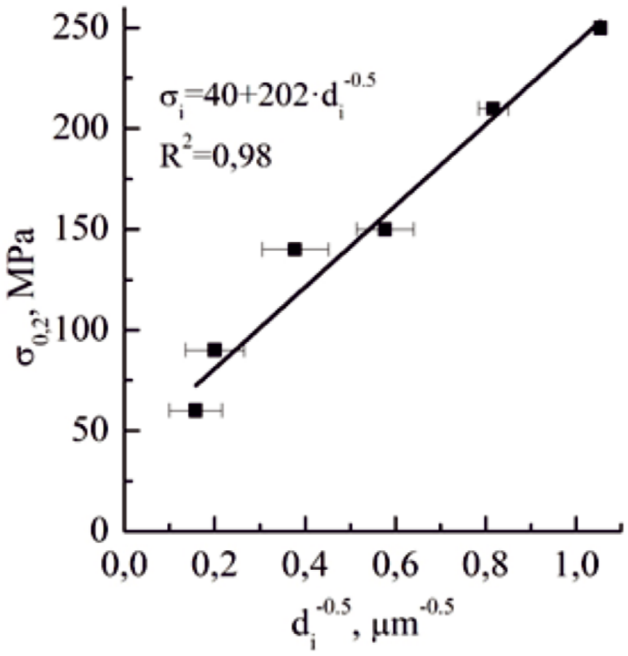


*Fig. 10*. Dependence of the yield strength $\sigma_{0.2}$ on the $d^{-1/2}$

where $\chi = 0.9$ is a constant characterizing the interaction between dislocations [38]; b = 0.321 nm is the magnitude of the Burgers vector for the most probable slip plane (the basal plane {0001} was considered as the most probable in this work); G = 17 GPa is the shear modulus for magnesium [39]; and <ρ> is the scalar dislocation density. The dislocation density values for magnesium in various structural states are presented in Table 1.

The value of the friction stress $\sigma_0$ in a single crystal was taken as $\sigma_0 = 14$ MPa, assuming that this value corresponds to the $\sigma_0$ for the equilibrium state of the CG alloy (annealed at 500 °C). The value of $\sigma_0$ for the CG state of the alloy was estimated as: $\sigma_0 = \sigma_{0.2} - \sigma_{dis} - \sigma_{gb}$, where $\sigma_{0.2} = 60$ MPa (experimental data); $\sigma_{dis} = 14$ MPa and $\sigma_{gb} = 32$ MPa (calculated data, Table 2).

The calculated values of $\sigma_{gb}$ and $\sigma_{dis}$ are presented in Table 2. For the CG alloy, the contribution from grain boundary strengthening was

Table 2

**Contributions of different strain hardening mechanisms in *MA20* alloy in various structural states**

| Alloy state | $\sigma_{dis}$, MPa | $\sigma_{gb}$, MPa | $\sigma_{0,}$ MPa | $\sigma_{total}$, MPa | $\sigma_{0,2}$, MPa |
|---|---|---|---|---|---|
| CG | 16 | 40 | 14 | 96 | 90 |
| FG | 35 | 117 | 14 | 166 | 140 |
| UFG | 69 | 202 | 14 | 286 | 250 |
| UFG + annealing at 200 °C | 47 | 202 | 14 | 263 | 230 |
| UFG + annealing at 250 °C | 38 | 165 | 14 | 217 | 210 |
| UFG + annealing at 300 °C | 31 | 76 | 14 | 122 | 140 |
| CG + annealing at 500 °C* | 14 | 32 | 14 | 60 | 60 |

* Note: CG + annealing at 500 °C – annealing of the initial coarse-grained state of the alloy at 500 °C for 8 hours to achieve a large grain size and relaxation of internal stresses.

≈40 MPa. The transition of the alloy to the FG state is accompanied by a substantial increase in $\sigma_{gb}$ – to 117 MPa, due to the significant refinement of the grain structure. The application of the combined SPD method, including abc press forging followed by rolling, forms a structure with a minimal grain size, which increases the value of grain boundary strengthening to 202 MPa. Annealing of the UFG alloy at 200 °C does not affect the value of $\sigma_{gb}$ compared to the UFG state without annealing, while maintaining an average grain size of 1 μm. Annealing at 250 and 300 °C promotes grain growth to 1.5 and 7 μm, respectively, and thereby reduces the grain boundary strengthening of the alloy to 165 and 76 MPa.

Annealing the CG (initial) alloy at 500 °C leads to the formation of a coarse-grained structure, whereby the contribution of grain boundary strengthening decreases to 32 MPa.

For the alloy in the CG state, the contribution of the dislocation strengthening mechanism was 16 MPa. In the FG state, the dislocation density increases, and the contribution of dislocation strengthening reaches 35 MPa. The UFG state is characterized by a high dislocation density and the maximum contribution of dislocation strengthening – 69 MPa. Annealing at 200 °C causes microstructural relaxation, a significant reduction in dislocation density, and, consequently, a decrease in $\sigma_{dis}$ to 47 MPa. Subsequent annealing at 250 and 300 °C leads to a reduction in $\sigma_{dis}$ to 38 and 31 MPa, which can be attributed to the activation of recovery processes and a decrease in the scalar dislocation density in the magnesium alloy samples. These results are consistent with the TEM data, which show a reduction in scalar dislocation density accompanied by a decrease in the contribution of dislocation strengthening. Simultaneously, annealing increases the average grain size, which reduces strength due to the decrease in both dislocation and grain boundary strengthening. During recrystallization annealing of the CG alloy at 500 °C, the dislocation density is minimal, and the calculated contribution of dislocation strengthening decreases to 14 MPa. The calculated values of $\sigma_{total}$ are in good agreement with the experimental data for $\sigma_{0.2}$ obtained from tensile mechanical tests.

Thus, the greatest contribution to the increase in strength of the magnesium alloy during combined SPD is made by the grain boundary strengthening mechanism, whose contribution due to grain refinement to 1 μm is $\sigma_{gb}$ = 202 MPa, and the dislocation strengthening mechanism with a contribution of $\sigma_{dis}$ = 69 MPa.

The presented calculated data are estimates but allow for the identification of the most significant contributions to the overall strengthening, and thereby, the primary strengthening mechanisms of the magnesium alloy. The dependencies of dislocation density and the calculated strengthening contributions on the average grain size for alloy MA20 are presented in Figure 11.

On the presented dependencies, a range with grain sizes from 1 to 7 μm can be identified, where a decrease in grain size is accompanied by a decrease in the values of $\sigma_{dis}$, $\sigma_{gb}$, $\sigma_{total}$ и $<\rho>$. This specified grain size range corresponds to the following alloy states: UFG, UFG (annealed at 200, 250, 300 °C), and FG.

Figure 12 presents graphs of the change in the intensity of the contributions to the flow stress.

On the specified dependencies, two regions with different intensities of change in $\sigma_{dis}$, $\sigma_{gb}$, $\sigma_{total}$, and $<\rho>$ can be indentified. In Region I, (1–7) μm, a sharp change in the contributions and dislocation density occurs

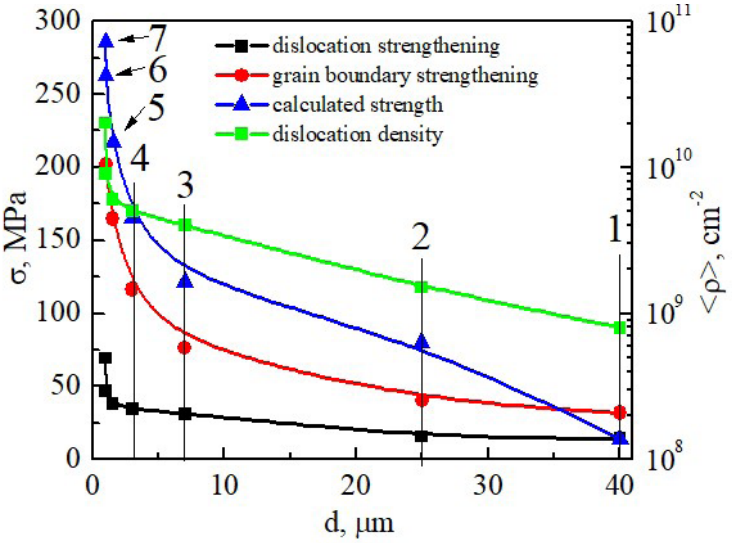


*Fig. 11.* Dependences of the contributions: $\boldsymbol{\sigma_{dis}}$, $\boldsymbol{\sigma_{grain}}$, $\boldsymbol{\sigma_{total}}$, and dislocation density on the grain size (sample numbers are presented in Table 1)

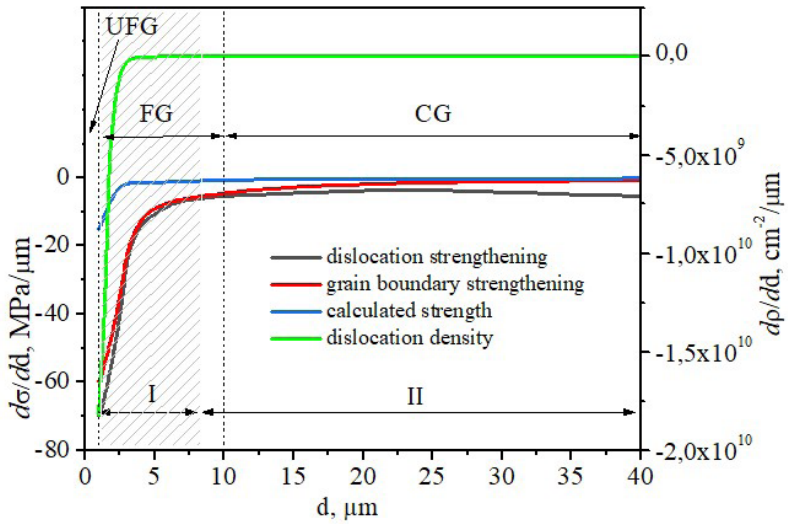


*Fig. 12.* Dependences of changes in the intensity of $\boldsymbol{d\sigma_{dis}/dd}$, $\boldsymbol{d\sigma_{grain}/dd}$, $d\boldsymbol{\sigma_{total}}/dd$, $d\boldsymbol{\rho}/dd$ on the grain size

for the UFG and FG states of the alloy. Region II can be characterized by a small change in the values $d\sigma_{dis}/d$d, $d\sigma_{gb}/d$d, $d\sigma_{total}/d$d, $d\rho/d$d, which corresponds to the CG state.

The change in the character of the dependencies is associated with the structural relaxation of the alloy during the transition from the UFG to the FG state due to recovery and defect annihilation processes, transformations of the structure inside grains and at grain boundaries, and the reorganization of the dislocation substructure during annealing. It is assumed that non-equilibrium grain boundaries, unlike equilibrium ones, form long-range stress fields that remain significant even over considerable distances and are capable of influencing the motion of intragranular dislocations. The low intensity of change in the contributions $d\sigma_{dis}/d$d, $d\sigma_{gb}/d$d, $d\sigma_{total}/d$d, and the density $d\rho/d$d for the CG state of the alloy suggests the formation of an equilibrium "sub-lattice" of grain boundary defects [19].

## Conclusion

1. The application of a combined SPD method, involving sequential abc press forging and multi-pass rolling of MA20 magnesium alloy, leads to the refinement of the grain structure to a UFG state (average

grain size: 1 μm), a substantial increase in yield and ultimate tensile strength ($\sigma_{0,2}$ = 250 MPa, $\sigma_{UTS}$ = 270 MPa) and a reduction in plasticity to 3%.

2. An assessment of the contributions from strain hardening mechanisms to the total yield strength $\sigma_{total}$ during combined SPD was conducted. It was shown that the greatest contribution to the strengthening of the UFG MA20 magnesium alloy is made by the grain boundary ($\sigma_{gb}$ = 202 MPa) and dislocation ($\sigma_{dis}$ = = 69 MPa) strengthening mechanisms.

3. Annealing at 200 °C preserves the UFG state in the MA20 magnesium alloy but, compared to the initial UFG state, promotes partial structural relaxation, a significant reduction in dislocation density, a 31% decrease in the $\sigma_{dis}$ contribution, an 8% decrease in $\sigma_{0.2}$, a 4% decrease in $\sigma_{UTS}$, and a 100% increase in plasticity.

4. For the studied alloy in the UFG and FG states, an interval of grain sizes equal to (1–7) μm was identified, corresponding to an abrupt change in the intensities of the dislocation density derivative ($d\rho/dd$), the contributions of the dislocation and grain boundary mechanisms to strain hardening ($d\sigma_{dis}/dd$, $d\sigma_{gb}/dd$), and the value of the total strengthening derivative $d\sigma_{total}/dd$.

## References


1. Yuan Y., Ma A., Gou X., Jiang J., Arhin G., Song D., Liu H. Effect of heat treatment and deformation temperature on the mechanical properties of ECAP processed ZK60 magnesium alloy. *Materials Science and Engineering: A*, 2016, vol. 677, pp. 125–132. DOI: 10.1016/j.msea.2016.09.037.

2. Chen S., Tseng K.-K., Tong Y., Li W., Tsai C.-W., Yeh J.-W., Liaw P.K. Grain growth and Hall-Petch relationship in a refractory HfNbTaZrTi high-entropy alloy. *Journal of Alloys and Compounds*, 2019, vol. 795, pp. 19–26. DOI: 10.1016/j.jallcom.2019.04.291.

3. Pan H., Yang C., Yang Y., Dai Y., Zhou D., Chai L., Huang Q., Yang Q., Liu S., Ren Y., Qin G. Ultra-fine grain size and exceptionally high strength in dilute Mg–Ca alloys achieved by conventional one-step extrusion. *Materials Letters*, 2019, vol. 237, pp. 65–68. DOI: 10.1016/j.matlet.2018.11.080.

4. Tong L.B., Chu J.H., Jiang Z.H., Kamado S., Zheng M.Y. Ultrafine-grained Mg-Zn-Ca-Mn alloy with simultaneously improved strength and ductility processed by equal channel angular pressing. *Journal of Alloys and Compounds*, 2019, vol. 785, pp. 410–421. DOI: 10.1016/j.jallcom.2019.01.181.

5. Xu C., Wang Z., Zhou L., Wang F., Wei Z., Mao P. Effect of element Ce on the strain rate sensitivity of Mg-Zn-Zr alloy. *Journal of Magnesium and Alloys*, 2025, vol. 13 (8), pp. 4005–4019. DOI: 10.1016/j.jma.2025.04.017.

6. Zhou Y.-L., Li Y., Luo D.-M., Ding Y., Hodgson P. Microstructures, mechanical and corrosion properties and biocompatibility of as extruded Mg–Mn–Zn–Nd alloys for biomedical applications. *Materials Science and Engineering: C*, 2015, vol. 49, pp. 93–100. DOI: 10.1016/j.msec.2014.12.057.

7. Yu K., Li W., Zhao J., Ma Z., Wang R. Plastic deformation behaviors of a Mg–Ce–Zn–Zr alloy. *Scripta Materialia*, 2003, vol. 48 (9), pp. 1319–1323. DOI: 10.1016/S1359-6462(03)00046-0.

8. Shunmugasamy V.C., AbdelGawad M., Sohail M.U., Ibrahim T., Khan T., Seers T.D., Mansoor B. In vitro and in vivo study on fine-grained Mg–Zn–RE–Zr alloy as a biodegradeable orthopedic implant produced by friction stir processing. *Bioactive Materials*, 2023, vol. 28, pp. 448–466. DOI: 10.1016/j.bioactmat.2023.06.010.

9. Volkova E.F. Some regular features of formation of phase composition in a magnesium alloy of the Mg – Zn – Zr – Y system. *Metal Science and Heat Treatment*, 2014, vol. 55 (9–10), pp. 477–482. DOI: 10.1007/s11041-014-9657-5.

10. Dobatkin S.V., Rokhlin L.L., Lukyanova E.A., Murashkin M.Y., Dobatkina T.V., Tabachkova N.Y. Structure and mechanical properties of the Mg-Y-Gd-Zr alloy after high pressure torsion. *Materials Science and Engineering: A*, 2016, vol. 667, pp. 217–223. DOI: 10.1016/j.msea.2016.05.003.

11. Minárik P., Král R., Pešička J., Chmelík F. Evolution of mechanical properties of LAE442 magnesium alloy processed by extrusion and ECAP. *Journal of Materials Research and Technology*, 2015, vol. 4 (1), pp. 75–78. DOI: 10.1016/j.jmrt.2014.10.012.

12. Merson D., Brilevsky A., Myagkikh P., Markushev M., Vinogradov A. Effect of deformation processing of the dilute Mg-1Zn-0.2Ca alloy on the mechanical properties and corrosion rate in a simulated body fluid. *Letters on Materials*, 2020, vol. 10 (2), pp. 217–222. DOI: 10.22226/2410-3535-2020-2-217-222.

13. Jin Z.-Z., Zha M., Wang S.-Q., Wang S.-C., Wang C., Jia H.-L., Wang H.-Y. Alloying design and microstructural control strategies towards developing Mg alloys with enhanced ductility. *Journal of Magnesium and Alloys*, 2022, vol. 10 (5), pp. 1191–1206. DOI: 10.1016/j.jma.2022.04.002.

14. Nie J.-F. Precipitation and hardening in magnesium alloys. *Metallurgical and Materials Transactions A*, 2012, vol. 43 (11), pp. 3891–3939. DOI: 10.1007/s11661-012-1217-2.

15. Shabana M.A., Bhattacharyya J.J., Niewczas M., Agnew S.R. Thermally activated nature of basal and prismatic slip in mg and its alloys. *Magnesium Technology 2021*. Cham, Springer, 2021, pp. 53–60. DOI: 10.1007/978-3-030-65528-0_9.

16. Yue Y., Wang J., Nie J.-F. Twin-solute, twin-dislocation and twin-twin interactions in magnesium. *Journal of Magnesium and Alloys*, 2023, vol. 11 (10), pp. 3427–3462. DOI: 10.1016/j.jma.2023.07.015.

17. Li L., Liu W., Qi F., Wu D., Zhang Z. Effects of deformation twins on microstructure evolution, mechanical properties and corrosion behaviors in magnesium alloys – A review. *Journal of Magnesium and Alloys*, 2022, vol. 10 (9), pp. 2334–2353. DOI: 10.1016/j.jma.2022.09.003.

18. Valiev R.Z., Islamgaliev R.K., Alexandrov I.V. Bulk nanostructured materials from severe plastic deformation. *Progress in Materials Science*, 2000, vol. 45 (2), pp. 103–189. DOI: 10.1016/S0079-6425(99)00007-9.

19. Glezer A.M., Kozlov E.V., Koneva N.A., Popova N.A., Kurzina I.A. *Plastic deformation of nanostructured materials*. CRC Press, 2017. ISBN 9781315111964.

20. Botkin A.V., Valiev R.Z., Volkova E.P., Khudododova G.D., Ebrahimi R. Effect of preliminary deformation on the formation of ultrafine-grained structure during equal channel angular pressing of magnesium alloys. *Fizicheskaya mezomekhanika = Physical Mesomechanics*, 2024, vol. 27, no. 4, pp. 63–72. DOI: 10.55652/1683-805X_2024_27_4_63-72. (In Russian).

21. Lukyanova E., Tarytina I., Tabachkova N., Dobatkina T., Martynenko N., Rybalchenko O., Rybalchenko G., Temralieva D., Andreev V., Ovchinnikova O., Andreeva N., Dobatkin S. The effect of rotary swaging on the structure and mechanical properties of Mg-Y-Gd-Zr alloys additionally alloyed with samarium. *Materials Today Communications*, 2025, vol. 43, p. 111857. DOI: 10.1016/j.mtcomm.2025.111857.

22. Luginin N., Eroshenko A., Khimich M., Prosolov K., Kashin A., Uvarkin P., Tolmachev A., Glukhov I., Panfilov A., Sharkeev Y. Severe plastic deformation of Mg–Zn–Zr–Ce alloys: advancing corrosion resistance and mechanical strength for medical applications. *Metals*, 2023, vol. 13 (11), p. 1847. DOI: 10.3390/met13111847.

23. Pekguleryuz M., Celikin M. Creep resistance in magnesium alloys. *International Materials Reviews*, 2010, vol. 55 (4), pp. 197–217. DOI: 10.1179/095066010X12646898728327.

24. Hirsch P.B., Howie A., Nicholson R.B., Pashley D.W., Whelan M.J., Marton L. Electron microscopy of thin crystals. *Physics Today*, 1966, vol. 19 (10), pp. 93–95. DOI: 10.1063/1.3047787.

25. Sun L., Wang Z., Zhou L., Wang F., Zhang W., Wei Z., Mao P. Effect of Ce on microstructure and corrosion behavior of as cast ZK60 alloy. *Materials Today Communications*, 2025, vol. 42, p. 111345. DOI: 10.1016/j.mtcomm.2024.111345.

26. Fruchart D., Skryabina N., de Rango P., Fouladvind M., Aptukov V. Severe plastic deformation by fast forging to easy produce hydride from bulk Mg-based alloys. *Materials Transactions*, 2023, vol. 64 (8), pp. 1886–1893. DOI: 10.2320/matertrans.MT-MF2022049.

27. Kappes M., Iannuzzi M., Carranza R.M. Hydrogen embrittlement of magnesium and magnesium alloys: a review. *Journal of the Electrochemical Society*, 2013, vol. 160 (4), pp. C168–C178. DOI: 10.1149/2.023304jes.

28. Zhang J., Yan S., Qu H. Stress/strain effects on thermodynamic properties of magnesium hydride: A brief review. *International Journal of Hydrogen Energy*, 2017, vol. 42 (26), pp. 16603–16610. DOI: 10.1016/j.ijhydene.2017.05.174.

29. Mezbahul-Islam M., Mostafa A.O., Medraj M. Essential magnesium alloys binary phase diagrams and their thermochemical data. *Journal of Materials*, 2014, vol. 2014, pp. 1–33. DOI: 10.1155/2014/704283.

30. Aljarrah M., Alnahas J., Alhartomi M. Thermodynamic modeling and mechanical properties of Mg-Zn-{Y, Ce} alloys: Review. *Crystals*, 2021, vol. 11 (12), p. 1592. DOI: 10.3390/cryst11121592.

31. Sharkeev Yu.P., Kozlov E.V. The long-range effect in ion implanted metallic materials: dislocation structures, properties, stresses, mechanisms. *Surface and Coatings Technology*, 2002, vol. 158–159, pp. 219–224. DOI: 10.1016/S0257-8972(02)00212-8.

32. Goldstein M.I., Litvinov V.S., Bronfin M.B. *Metallofizika vysokoprochnykh splavov* [Metal physics of high-strength alloys]. Moscow, Metallurgiya Publ., 1986. 312 p. (In Russian).

33. Gleiter H. Nanostructured materials: basic concepts and microstructure. *Acta Materialia*, 2000, vol. 48 (1), pp. 1–29. DOI: 10.1016/S1359-6454(99)00285-2.

34. Raynor G.V. *The physical metallurgy of magnesium and its alloys*. New York, Pergamon Press, 1959. 531 p.

35. Gong W., Zheng R., Harjo S., Kawasaki T., Aizawa K., Tsuji N. In-situ observation of twinning and detwinning in AZ31 alloy. *Journal of Magnesium and Alloys*, 2022, vol. 10 (12), pp. 3418–3432. DOI: 10.1016/j.jma.2022.02.002.

36. Prasad N.S., Naveen Kumar N., Narasimhan R., Suwas S. Fracture behavior of magnesium alloys – Role of tensile twinning. *Acta Materialia*, 2015, vol. 94, pp. 281–293. DOI: 10.1016/j.actamat.2015.04.054.

37. Balog M., Krížik P., Školáková A., Švec P., Kubásek J., Pinc J., de Castro M.M., Figueiredo R. Hall-Petch strengthening in ultrafine-grained Zn with stabilized boundaries. *Journal of Materials Research and Technology*, 2024, vol. 33, pp. 7458–7468. DOI: 10.1016/j.jmrt.2024.11.132.

38. Oppedal A.L., El Kadiri H., Tomé C.N., Kaschner G.C., Vogel S.C., Baird J.C., Horstemeyer M.F. Effect of dislocation transmutation on modeling hardening mechanisms by twinning in magnesium. *International Journal of Plasticity*, 2012, vol. 30–31, pp. 41–61. DOI: 10.1016/j.ijplas.2011.09.002.

39. Ganeshan S., Shang S.L., Wang Y., Liu Z.-K. Effect of alloying elements on the elastic properties of Mg from first-principles calculations. *Acta Materialia*, 2009, vol. 57 (13), pp. 3876–3884. DOI: 10.1016/j.actamat.2009.04.038.

## Conflicts of Interest

The authors declare no conflict of interest.